Bioactive Materials 18 (2022) 446–458

Contents lists available at ScienceDirect

Bioactive Materials

journal homepage: www.keaipublishing.com/en/journals/bioactive-materials

A facile and general method for synthesis of antibiotic-free protein-based hydrogel: Wound dressing for the eradication of drug-resistant bacteria and biofilms

Jiang Ouyang [a,b], Qingyue Bu [a], Na Tao [d], Mingkai Chen [a], Haijun Liu [b], Jun Zhou [b], Jinggong Liu [e], Bo Deng [a], Na Kong [b], Xingcai Zhang [c,***], Tianfeng Chen [a,**], Yihai Cao [f], Wei Tao [b,*]

[a] The First Affiliated Hospital, Department of Chemistry, Jinan University, Guangzhou, 510632, China
[b] Center for Nanomedicine and Department of Anesthesiology, Brigham and Women's Hospital, Harvard Medical School, Boston, MA, 02115, USA
[c] John A. Paulson School of Engineering and Applied Sciences, Harvard University, Cambridge, MA, 02138, USA
[d] College of Chemistry and Chemical Engineering, Central South University, Changsha, Hunan, 410083, China
[e] The Second Affiliated Hospital of Guangzhou University of Chinese Medicine, Guangdong Provincial Academy of Chinese Medical Sciences, Guangzhou, 510006, China
[f] Department of Microbiology, Tumor and Cell Biology, Karolinska Institute, Stockholm, 171 77, Sweden

ARTICLE INFO

Keywords:
THPS
Protein hydrogel
Bacterial resistance
Anti-Biofilm
Wound dressing

ABSTRACT

Antibacterial protein hydrogels are receiving increasing attention in the aspect of bacteria-infected-wound healing. However, bacterial drug resistance and biofilm infections lead to hard healing of wounds, thus the construction of biological agents that can overcome these issues is essential. Here, a simple and universal method to construct antibiotic-free protein hydrogel with excellent biocompatibility and superior antibacterial activity against drug-resistant bacteria and biofilms was developed. The green industrial microbicide tetrakis (hydroxymethyl) phosphonium sulfate (THPS) as cross-linking agent can be quickly cross-linked with model protein bovine serum albumin (BSA) to form antibacterial hydrogel through simple mixing without any other initiators, subsequently promoting drug-resistance bacteria-infected wound healing. This simple gelatinization strategy allows at least ten different proteins to form hydrogels (e.g. BSA, human serum albumin (HSA), egg albumin, chymotrypsin, trypsin, lysozyme, transferrin, myohemoglobin, hemoglobin, and phycocyanin) under the same conditions, showing prominent universality. Furthermore, drug-resistance bacteria and biofilm could be efficiently destroyed by the representative BSA hydrogel (B-Hydrogel) with antibacterial activity, overcoming biofilm-induced bacterial resistance. The in vivo study demonstrated that the B-Hydrogel as wound dressing can promote reepithelization to accelerate the healing of methicillin-resistant staphylococcus aureus (MRSA)-infected skin wounds without inducing significant side-effect. This readily accessible antibiotic-free protein-based hydrogel not only opens an avenue to provide a facile, feasible and general gelation strategy, but also exhibits promising application in hospital and community MRSA disinfection and treatment.

1. Introduction

Bacterial wound infection generally not only prolongs wound healing, but also may cause other serious problems, such as systemic infections, sepsis, organ failure, and even death [1–3]. Although the advent of antibiotics has slowed the progression of bacterial infections to some extent, the overuse of antibiotics has led to the emergence of antibiotic-resistant strains of pathogenic bacteria that are increasingly spreading in communities and hospitals [4,5]. Additionally, persistent bacterial wound infection is usually mediated by the highly organized structure of bacterial biofilms, which are the communities of bacteria that irreversibly adheres to the material or tissue surface and are coated

Peer review under responsibility of KeAi Communications Co., Ltd.
* Corresponding author.
** Corresponding author.
*** Corresponding author.
E-mail addresses: xingcai@mit.edu (X. Zhang), tchentf@jnu.edu.cn (T. Chen), wtao@bwh.harvard.edu (W. Tao).

https://doi.org/10.1016/j.bioactmat.2022.03.033
Received 25 January 2022; Received in revised form 11 March 2022; Accepted 22 March 2022

with self-generated extracellular polymers (EPS) [6,7]. The EPS can prevent bacteria in biofilms from being attacked by antibiotics and the host's innate immune cells, providing a favorable confined-space for drug-resistant strains arising, which also results in great challenges in the clinical treatment of biofilms [6].

Although the antibacterial hydrogels with structural diversity developed in recent years have high oxygen permeability and superior water swelling, providing new possibilities for the prevention and treatment of bacterial infectious diseases, most of these hydrogels generally exploit antibiotics to fight against bacterial infection [2,8–10], which will inevitably cause bacterial resistance. Furthermore, these antibacterial hydrogels often can only eliminate planktonic microorganisms rather than causing the complete eradication of the formed biofilms, greatly restricting their use in bacterially infected wounds. Some antimicrobial hydrogels integrate metal fungicides such as silver nanoparticles [7,11–14], zinc oxide nanoparticles [15], or gold nanoparticles [16,17] into the hydrogel networks, which exhibit good antibacterial activity against drug-resistant bacteria and certain anti-biofilm activity, but some of them also suffer the certain risk of causing metal cytotoxicity. Exploiting inherent organic fungicides including cationic polymers [18,19], cationic peptides [20], or cationic small molecules [21,22] may be a feasible solution for the development of long-term intrinsic antibacterial hydrogels against drug-resistant bacteria and biofilm. However, synthetic cationic polymers and peptides usually require complex operations and high costs, and their poor cell and tissue affinities as well as potential immunogenicity also seriously restrict their extensive applications in antibacterial dressing. Therefore, it is urged to explore bactericidal hydrogels for the elimination of drug-resistant bacteria and biofilms, which are featured with low costs, simple synthesis, strong and persistent antibacterial activity while being free of antibiotics and toxic reagents.

Microbicide tetrakis (hydroxymethyl) phosphonium sulfate (THPS), a low-cost phosphine exhaust byproduct of cationic phosphonium salt with similar antibacterial activity to the above cationic polymers or cationic peptides [23], which can significantly suppress the growth of fungi algae and bacteria, and can be quickly degraded into completely harmless substances after use [24–27]. In addition, similar to the antibacterial mechanisms of cationic polymers and peptides, THPS also

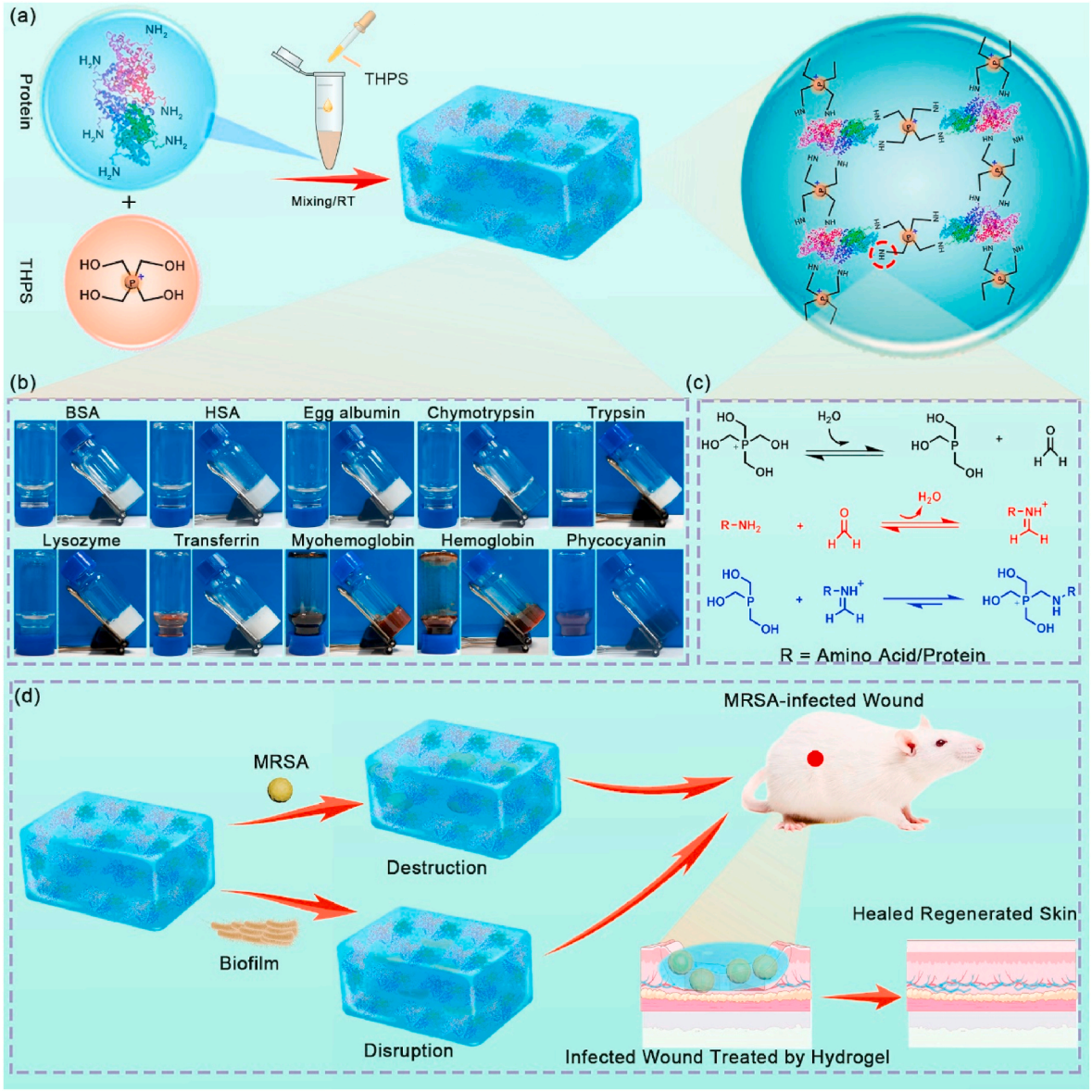

Fig. 1. (a) The formation and crosslinking of antibiotic-free protein-based hydrogel. (b) Digital photos of different proteins before and after gelation. (c) Possible mechanism of THPS reaction with the amino group in proteins. (d) The antibacterial ability of B-Hydrogels and their applications in the treatment of MRSA-infected wounds.

possesses an excellent ability to destroy bacterial biofilms and hardly causes bacterial resistance during the antibacterial process [28,29]. Given these merits, THPS can serve as a perfect substitute for antibiotics, metal fungicides, cationic polymers and peptides. However, few studies about THPS-based hydrogels used as dressings against drug-resistant bacteria and biofilms have been reported.

Protein is the scaffold and main substance that constitute human tissues and organs, which plays an important role in human life activities [30]. As a natural polymer derived from the organism, protein is rich in amino acids, which can form β-sheet-rich fibrils to further self-assemble and twine under appropriate conditions for the formation of three-dimensional hydrogels through hydrophobic effects, electrostatic interactions, or hydrogen bonding [31,32]. Owing to the easy manipulability of bioactivity and ready availability, the protein-based hydrogel has attracted extensive attention in biomedicine [30,31,33,34]. Herein, we exploited THPS and model proteins (e.g., BSA) to construct antibiotic-free antibacterial hydrogels by simply mixing the two precursors uniformly at room temperature for MRSA-infected wound healing treatment (Fig. 1). Because BSA composes of many various amino acids and contains both α-helix and β-sheet in its secondary structure, which could react with THPS through Mitchell reaction to form hydrogel with excellent biocompatibility. This readily available gelatinization strategy can also be applied to other different proteins, such as HSA, egg albumin, chymotrypsin, trypsin, lysozyme, transferrin, myohemoglobin, hemoglobin, and phycocyanin (Fig. 1b), showing good universality. Notably, the constructed antibiotic-free B-Hydrogel not only displayed strong and long-lasting bactericidal activity against MRSA and *Staphylococcus aureus* (SA), but also could dilapidate the bacterial biofilms to avoid causing biofilm-induced bacterial resistance. With the assistant of B-Hydrogel, the MRSA-infected mice wound could recover quickly without generating obvious side effects (Fig. 1d). Therefore, this readily accessible protein hydrogel not only provides a reference paradigm for the construction of protein-based hydrogel, but also shows the great potential to fight against drug-resistant bacterial infection and bacterial biofilms.

2. Materials and methods

2.1. Materials

Bovine serum albumin (BSA), human serum albumin (HSA), egg albumin, chymotrypsin, trypsin, lysozyme, transferrin, myohemoglobin, hemoglobin, phycocyanin, propidium iodide (PI), and calcein-AM were brought from Sigma-Aldrich. Phalloidin-FITC, 4′,6-diamidino-2-phenylindole (DAPI), DMEM culture medium, foetal bovine serum (FBS), trypsin-EDTA, phosphate-buffered saline (PBS) (pH 7.4), and penicillin-streptomycin solution were purchased from Thermo Fisher. Luria−Bertani (LB) broth medium, agarose, Lactase Dehydrogenase (LDH) kit and Cell Counting Kit-8 (CCK-8) kit were brought from Beyotime Biotechnology (Shanghai, China). THPS (ca. 75 in Water, MW 406.28) solution was brought from Aladdin. *Staphylococcus aureus* (*S. aureus*, SA, ATCC25923) and methicillin-resistant staphylococcus aureus (MRSA, ATCC43300) strains were purchased from HuanKai Microbial. Deionized water (18.2 MΩ cm) was used in whole experiments.

2.2. Characterizations

UV–vis spectrophotometer (UH4150, HITACHI, Japan) was used to measure the UV–vis absorbance. PerkinElmer Spectrum One Instrument (America) was employed for fourier transform infrared spectra (FT-IR) spectra. Rheological measurements were performed using a rheometer (AR 2000ex, TA Instruments, USA). Fluorescence imaging is performed using a Lycra confocal laser focusing microscope (LSM800, ZEISS, Germany). A NOVA nano SEM230 (FEI, USA) was used for scanning electron microscopy (SEM) imaging. The optical density (OD) value was recording using a microplate reader (BioTek, USA). Phosphorus spectrometry (PS) was performed on a proton NMR spectrum (Bruker Daltonics, Germany). TEM imaging was performed on a transmission electron microscopy (TEM; JEOL, JEM-2100F, 200 kV). Zeta Potential was determined using a Malvern Zetasizer Nano-ZS instrument (ZEN3600, Malvern Instruments). A Raman microspectrometer (Jobin Yvon LabRam-010, France) (excitation wavelength: 633 nm) was used for Raman scattering.

2.3. Preparation of B-Hydrogels

Take different volumes (70, 60, 50, 40, 30, 20 μL) of THPS solution (w/w_0 75%) and dilute to 1 mL. Then, 50 μL diluted THPS solution with different concentration was first mixed with 250 μL deionized water, followed by 200 μL of 200 mg mL^{-1} BSA solution. Shake the mixture well and let it stand for a while, then a transparent B-Hydrogel was obtained about 50 min later. HSA hydrogel and egg albumen hydrogel were prepared as the same way mentioned above, with the only difference being that the protein source was changed.

2.4. Rheological studies of B-Hydrogel

Rheological measurements were performed on a rheometer. Hydrogel samples were placed on the rheometer stage, a dynamic frequency sweeping from 0.01 to 100 Hz under the strain at 1% at 25 °C. Viscosity of the hydrogel with increasing shear rate from 0.01 to 10 rad s^{-1} by continuous flow experiment was conducted under the strain at 1% at 25 °C. Dynamic modulus of hydrogel under increasing strain with a fixed frequency of 1 Hz at 25 °C.

2.5. Antimicrobial testing of B-Hydrogel

Bacteria of SA (ATCC25923) and MRSA (ATCC43300) strains were employed as the model of bacteria to investigate the antibacterial activity of B-Hydrogel in our experiment. Before the experiment, MRSA and SA bacteria were incubated in liquid LB culture medium for 24 h at 37 °C, then collected at logarithmic phase through centrifugation at 3500 rpm s^{-1} for 4 min and wash twice with sterile PBS. The collected bacteria were resuspended into the liquid medium with different volume to obtain bacterial suspensions with different concentrations. For time-dependent antimicrobial assay, bacteria solution was divided into 4 groups: 1) control, 2) BSA, 3) THPS, and 4) B-Hydrogel (THPS: 0.3%), then the bacteria (500 μL) were received corresponding treatments, and the final bacterial density was 1×10^6 CFU mL^{-1} were mixed with BSA hydrogel. Afterwards, the absorbance of bacterial solution at 600 nm (OD_{600}) at different time intervals was monitored to observe bacterial growth. Additionally, after 12 h incubation, part of the bacterial solution in various groups was taken out and diluted to perform agar plate cloning experiment to quantify bacterial survival and density. The remaining bacteria were continued to culture. To study the integrity of the bacterial membrane, the same treatments as above were performed towards the SA and MRSA bacteria for 12 h, and then the treated bacteria were further stained with PI and calcein-AM for 1 h. Afterwards, collecting the SA and MRSA via centrifugation, and using PBS to wash them twice for subsequent fluorescence imaging.

2.6. LDH release assay

SA and MRSA bacteria (1×10^6 CFU mL^{-1}) were received the treatments as the above mentioned at 37 °C for 12 h. Subsequently, the bacterial solution was centrifuged for 5 min (5000 rpm s^{-1}) to collect the supernatants for LDH release measurement via LDH kit. Based on the following equation (1), the release rate of LDH can be calculated:

$$\text{LDH release rate } (\%) = (C - C_0)/(C_T - C_0) \times 100\% \quad (1)$$

C and C_0 are the release of LDH from bacteria treated with various

groups and untreated bacteria, respectively. C_T represents the total release of LDH from bacteria with 1% Triton X-100 treatment.

2.7. SEM and TEM imaging of bacterial morphology

Both the SA and MRSA bacteria with or without B-Hydrogel treatment were collected via centrifugation at 4000 rmp s^{-1} for 5 min, then the obtained bacteria were washed with PBS twice. Afterwards, the bacteria were fixed with paraformaldehyde at room temperature for 2 h. After wash with PBS, the bacteria were further dehydrated by a series of 10, 25, 50, 75, 90, and 100% ethanol solution for 15 min with each step. After the completion of the last step, bacteria suspension was dropped onto the cover glass. After drying through freeze-dried at the room temperature, SEM was used for bacterial morphology imaging. For TEM imaging, the fixed bacteria were further immobilized with osmium acid (OsO_4) for 2 h and then washed three times with PBS. Subsequently, the bacteria were dehydrated with successive ethanol (50%, 70%, 90%), mixture of ethanol and acetone (90%: 90%), and acetone (90%, 100%) solution for 10 min each step. Finally, the bacterial were further dehydrated with the mixture of acetone (100%) and embedding medium (1: 1) for 2 h. Then, the dehydrated bacteria were further embedded in epoxy resin and stained with uranyl acetate (3%) after sectioned, and imaging with TEM.

2.8. Cytotoxicity assay and cell fluorescence imaging

The cytotoxicity of B-Hydrogel was evaluated by HUVECs and NIH-3T3 cells using CCK-8 kit. The cells were incubated using DMEM culture medium with penicillin–streptomycin (1%) and FBS (10%) at the atmosphere of 37 °C and 5% CO_2. Both the HUVECs and NIH-3T3 cells were seeded into 96-wells plate at the density of 1×10^5 cells/well. After overnight incubation, the cells were co-incubated with B-Hydrogel (traces) for another 24. Finally, removing the hydrogel and medium, and adding fresh medium containing CCK-8 into corresponding wells for another 2 h incubation before measuring the value of OD_{450}.

For cell fluorescence imaging, after incubation with hydrogel for 24 h, the cells were stained with Phalloidin-FITC for 30 min. Afterwards, DAPI solution was added into cells for another 10 min incubation. Washing the cells with PBS for twice and imaging the cells using laser scanning confocal microscopy.

2.9. Biofilm fluorescence imaging

Both the SA and MRSA bacteria in logarithmic phase were seeded in 24-well plate containing coverslips and incubated in LB medium. After 24 h culture, removing the medium in each well, and washing the formed biofilms with PBS for three times carefully to remove floating bacteria. Afterwards, LB medium (0.5 mL) was added into every well, and addition of B-Hydrogel into medium subsequently. After 12 h culture, removing the medium and hydrogel, and adding the Calcein-AM and PI to stain the biofilms. After 30 min staining, the biofilms were imaged using a laser confocal microscopy.

To further investigate the anti-biofilm activity of B-Hydrogel, the biofilms on the coverslips were stained with crystal violet after treated with B-Hydrogel. Dissolving the crystal violet using ethanol and measuring the absorbance at 590 nm (OD_{590nm}) by microplate reader to quantify the biofilm mass. Based on equation (2) to calculate the relative biofilm mass:

$$\text{Biofilm mass } (\%) = m_0/m_T \times 100\% \quad (2)$$

Where, m_0 and m_T were the OD_{590nm} values with or without B-Hydrogel treatment, respectively.

2.10. Animal experiments

Female BALB/c mice (6 weeks) were purchased from Charles River. All animal experiments were executed according to NIH's Guide for the Care and Use of Laboratory Animals under sterile conditions at the animal facility of Brigham and Women's Hospital. All experimental protocols were approved under the guidelines of the Institutional Animal Care and Use Committees at Harvard Medical School.

To establish the mice model of wound infection, the mice were first anesthetized with sodium pentobarbital, followed by sterile scissors to create a round wound (diameter: 8 mm) on the mice's back. To induce skin infection, 100 μL PBS containing MRSA (5×10^8 CFU mL^{-1}) was dropped onto the wound. Then, PBS solution was used to wash the infected wound twice to remove the excess bacteria. Subsequently, the infected mice were divided into 4 groups and received corresponding treatments: Control (G1); BSA (G2); THPS (G3); and B-Hydrogel (G4). After treatments, the wound areas of mice were recoded and taken photograph every 2 d. On day 4, 8 and 12, some representative mice in each group were sacrificed, and collecting the wound skin for immunofluorescence histology and histological staining.

3. Results and discussion

3.1. Fabrication and characterizations of B-Hydrogel

The manufacturing process of B-Hydrogel is shown in Fig. 1a. 10 wt % BSA solution (450 μL) was mixed with different concentrations of THPS diluent (50 μL) to obtain the hydrogels with different mechanical properties ranging from transparent to translucent to white (Fig. 2a). No gelation was found when the THPS concentration was lower than 0.2% (v/v_0) (Fig. S1). Similar phenomenon was also observed in HSA and egg albumin that are structurally similar to BSA (Figs. S2 and S3). Since the gelation time is crucial to the biological application of hydrogels, we then investigated the gelation time of B-Hydrogel. When the THPS solution was not less than 0.3%, the gelation time was about 50 min (Table S1), and the gelation time decreased slightly with the increase of THPS solution. However, the gelation time increased significantly when the concentration of the THPS solution was less than 0.3%. When the concentration of THPS was 0.2%, the gelation time was more than 4 h. Similar gelation time trends were also observed in HSA and egg albumin, confirming the universality of gelation processes in these hydrogels. To further prove the formation of B-Hydrogel, corresponding frequency-dependent oscillatory rheology was tested. As shown in Fig. 2b, the storage modulus (G′) obviously surpassed the loss modulus (G″) throughout the whole frequency range even the concentration of THPS at 0.2%, confirming the formation of a hydrogel. Notably, the G′ and G″ values of B-Hydrogel apparently enhanced with the increase of THPS concentration (Fig. 2b), demonstrating the enhancement of the rheological properties of B-Hydrogel. Furthermore, the strain-induced damage property of the B-Hydrogel to evaluate their responsive behaviors under external strains was performed through rheological strain sweep measurement. When the frequency and temperature were fixed at 1 Hz and 25 °C, the gel-to-sol transition point occurred at 35.34% in the strain range of 0.01%–1000% at the THPS concentration of 0.2%, indicating the hydrogel collapsed (Fig. S4). The gel-to-sol transition point also increased over the THPS concentration, demonstrating the excellent shear-thinning of B-Hydrogel. Subsequently, the microstructures of the B-Hydrogel were observed by scanning electron microscopy (SEM). As shown in Fig. 2c, an apparent interpenetrating network and porous structures of freeze-dried B-Hydrogel were observed, and with the increase of THPS concentration, pore diameter gradually decreased, indicating that the hydrogel structure became denser. Similar morphologies, structures and phenomena were also observed in HSA and egg albumin hydrogels (Figs. S5 and S6). The EDS mapping confirmed the presence of phosphorus element (P) in the hydrogel (Fig. 2d), which accounted for about 2% of the whole gel (Fig. S7), proving the cross-

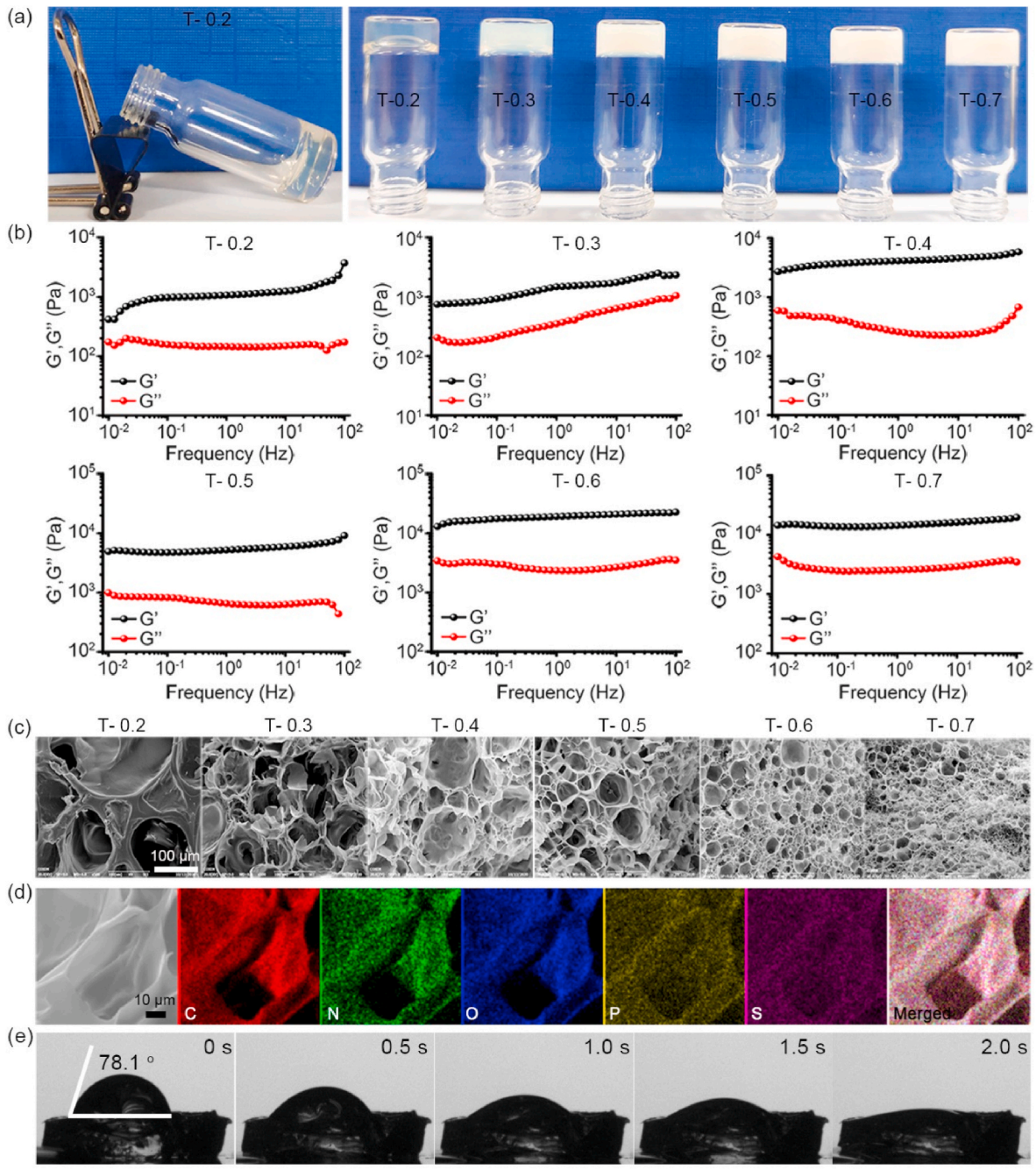

Fig. 2. (a) Digital photograph, (b) Dynamic rheological behavior, and (c) SEM images of B-Hydrogel with different concentration of THPS (T- 0.2 to T- 0.7 represent THPS concentration of 0.2%–0.7%). (d) Element mapping of B-Hydrogel. (e) Water contact angle of B-Hydrogel.

linking between THPS and BSA. Subsequently, the wettability and adsorption ability of B-Hydrogel were investigated via water contact angle. As shown in Fig. 2e, a droplet of water was almost completely adsorbed by B-Hydrogel within 2.0 s, demonstrating its superior wettability and adsorption ability, which is conducive to the subsequent wound healing. Taken together, all of these results demonstrate that the high-performance B-Hydrogel can be successfully constructed by using this simple approach that can also be applied to other proteins.

3.2. The mechanism of B-Hydrogel formation

According to a previous report [35], β-[tris(hydroxylmethyl) phosphino] propionic acid (THPP) could react with primary and secondary amines via a Mannich-type reaction to form polypeptide-based biomaterials. Owing to the similarity in structure, THPS has also been considered for Mannich-type reaction with primary and secondary amines, which have been applied to react with polyamides for antibacterial membranes formation [36]. Therefore, we speculate that amine-rich BSA was also cross-linked with THPS to form hydrogels through the Mannich-type reaction. Because the Mannich-type reaction is mainly a process in which the active hydrogen of formaldehyde is replaced by an amine to form a Mannich base or immonium ion [37]. The formed Mannich base or immonium ion further reacts with the THPS derivative (tris(hydroxymethyl)phosphine) to generate the amine coupling, resulting in the formation of hydrogel (Fig. 1c). To test this hypothesis, the hydrolysate of THPS was first detected, and it was found that the content of formaldehyde in THPS aqueous solution gradually increased with the increase of THPS concentration (Fig. 3b), proving the

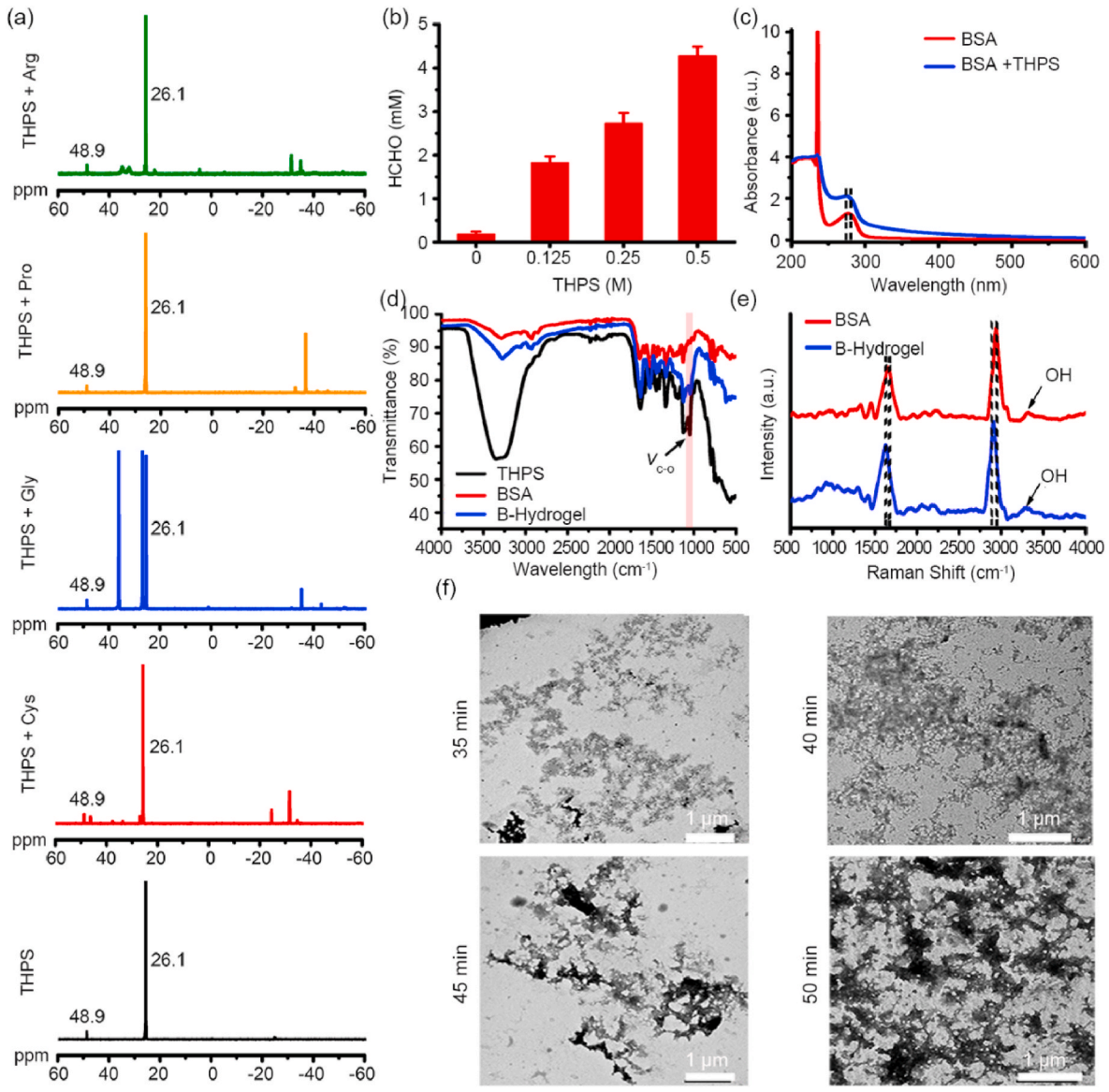

Fig. 3. (a) ^{31}P NMR of THPS alone compared to THPS react-ed with cystine (Cys), glycine (Gly), proline (Pro), and arginine (Arg). (b) Positive correlation between the amount of formaldehyde generation spontaneously for THPS in aqueous solution and its con-centration. (c) UV absorption of BSA before and after reaction with THPS. (d) FTIR spectra of THPS, BSA and B-Hydrogel. (e) Raman spectra of BSA and B-Hydrogel. (f) TEM images of the reac-tion process of BSA and THPS at different time points.

existence of formaldehyde in the hydrolysate. The ^{31}P NMR confirmed the existence of tris(hydroxymethyl)phosphine (Fig. 3a), confirming the mechanism proposed above. To further confirm the potential reaction mechanism, the lysine, glycine, or proline were employed to check whether the THPS would react with primary and secondary amines of BSA. As expected, there were two different states of phosphorus for the THPS stock solution in the ^{31}P NMR, which corresponded to THPS (48.9 ppm) and tris(hydroxymethyl)phosphine (26.1 ppm), respectively (Fig. 3b). After reaction with arginine (containing both primary and secondary amines), glycine (containing primary amine), proline (containing secondary amine), and cystine (containing primary amine and disulfide bond), more phosphorus signal peaks appeared for all the ^{31}P NMR and showed a phenomenon of shifting upfield (Fig. 3b), suggesting the state of more electron-rich. These results demonstrate that both primary and secondary amines can react with THPS, while the other active bonds would have no significant influence on this reaction, which also predicts that THPS would react with BSA. The variation of UV absorption peak before and after BSA solution and THPS reaction further confirmed the above inference. The absorbance peak at 275 nm of BSA solution exhibited an obvious blue shift after mixing with THPS for 35 min (Fig. 3c), suggesting the reaction of BAS with THPS. Compared with BSA, a new FTIR band at 1050 cm^{-1} for the BSA hydrogel was observed (Fig. 3d), corresponding to the THPS, which is ascribed to $\nu_{c\text{-}o}$ of a primary alcohol, proving the cross-linking of THPS and BSA. The Raman spectra also confirmed the cross-linking of THPS and BSA, an obvious blue shift for the Raman characteristic peaks was observed, while the –OH peak of B-Hydrogel was obviously stronger than BSA (Fig. 3e). All of these results prove that THPS and BSA could be cross-linked to form hydrogels according to the mechanism shown in the schematic diagram (Fig. 1c). Subsequently, the formation process of B-Hydrogel was further investigated by TEM. As shown in Fig. 3f, sporadic microaggregates could be found after mixing of THPS and BSA solution for 35 min. After 40 min of reaction, these microaggregates gradually grew larger, and tended to form a network. With the increase of reaction time, the formed interpenetrating network gradually changed from sparse to dense, ultimately forming a gel network. Overall, through Mannich-type reaction,

THPS and BSA can gradually develop from microaggregate structure to a network structure and form the hydrogel.

3.3. In vitro antibacterial performance

We then moved forward to investigate the bactericidal activity of B-Hydrogel. Gram-positive bacteria SA and MRSA were selected as the common model bacteria and drug-resistant model bacteria to evaluate the antibacterial activity of B-Hydrogel. After different treatments, the optical density at 600 nm (OD_{600}) of bacteria in different treatments was measured to assess the bacterial activity. As shown in Fig. 4a, there was no obvious influence on the bacterial growth for the BSA solution, which was nearly the same as the control group. In comparison, both the THPS solution and B-Hydrogel almost completely inhibited MRSA growth, which was attributed to the strong bactericidal effect of THPS. The bacteria turbidity image also confirmed the above result (Fig. 4b). Notably, the same antibacterial phenomenon of B-Hydrogel against SA was observed in the same experimental condition, demonstrating that the BSA hydrogel had superior antibacterial activity against both drug-resistant bacteria and common bacteria. To further prove the antibacterial effect of B-Hydrogel, the agar plate assay was executed. Almost no bacterial colonies for both MRSA and SA were observed on the agar plates after treatment with THPS solution and B-Hydrogel, however, there was a large number of bacteria survived in the BSA and control groups (Fig. 4c). Inhibition rings test results also suggested that there were obvious antibacterial rings with the zone of inhibition (ZOI) of about 1.5 and 1.0 cm for the MRSA and SA after treated with B-Hydrogel, respectively (Fig. 4d), indicating a superior sterilization effect. Additionally, the antibacterial capacities of the B-Hydrogel against different concentrations of MRSA and SA were systematically assessed. As displayed in Fig. 4e, the B-Hydrogel could almost completely suppress the proliferation of MRSA and SA when the concentration of MRSA and SA was less than 10^9 CFU mL^{-1}, and there was still a certain bacteriostatic effect for the B-Hydrogel, even when the bacteria concentration was 10^9 CFU mL^{-1}. All these results showed that the B-Hydrogel possessed the prominent antibacterial activity against common and resistant bacteria.

3.4. Antibacterial mechanism of B-Hydrogel

Next, we investigated the possible mechanism underlying the antimicrobial effects of B-Hydrogel by detecting the membrane integrity of bacteria using SEM. As shown in Fig. 4f, the complete spherical structure and smooth surface were observed in the normal bacteria, while agglomerate and shapeless bacteria with obvious surface collapse were found due to the serious destruction of the cell membranes after being treated with B-Hydrogel. The bio-TEM was utilized to further confirm the above results. For the normal bacteria, the contour of the bacterial cell membrane/wall was clearly visible and an intact morphology was observed (Fig. 4g). However, after the bacteria were treated with B-Hydrogel, they almost completely lost their bacterial membrane/wall and a distinct structural disruption was found (Fig. 4g). Moreover, upon the treatment with the B-Hydrogel, the leakage of lactate dehydrogenase (LDH) in MRSA and SA was 96% and 94.8%, respectively, demonstrating the severe damage of the bacterial cell membrane/wall (Fig. S8). Based on the above results, we speculated the possible antibacterial mechanism of B-Hydrogel was that the THPS ingredient with positively charged in B-Hydrogel could effectively adsorb the negatively charged bacterial lipid membrane through electrostatic interaction, resulting in the gradual lysis of membrane and causing bacterial apoptosis eventually. Furthermore, the free THPS released from the B-Hydrogel also destroyed bacteria through their bactericidal abilities. The live/dead staining assay also verified this contact-killing mechanism. Propidium iodide (PI), a membrane-impermeable indicator, can only penetrate the impaired bacterium, binding with DNA by embedding base pairs with almost no sequence bias to produce the red fluorescence, which is applied to detect bacterial membranes damage [4,33]. Meanwhile, using calcein-AM to stain live bacteria and emit green fluorescence for examining the integrity of bacterial cell membranes. For the bacteria with THPS or B-Hydrogel treatment, almost all of the bacteria were stained with red fluorescent PI, indicating the destruction of bacterial membrane structure (Fig. 5a). In contrast, almost all the bacteria in BSA solution and control groups emitted green fluorescence, demonstrating the structural integrity of the bacterial cell membrane. These results also demonstrating that THPS could induce membrane injury, thereby causing increased membrane permeability of bacteria, accounting for the antimicrobial mechanism of B-Hydrogel.

3.5. Anti-biofilms activity and biocompatibility of B-Hydrogel

According to previous report, 80% of bacterial infections are associated with the formation of bacterial biofilms [38–41]. Compared with planktonic bacteria, the resistance of bacterial membranes to antibiotics is tens to thousands of times higher, which is the main cause of bacterial drug resistance at present [42,43]. Therefore, owing to the protection afforded by the substrate formed during their growth, biofilms are more difficult to eliminate. To further confirm their superior antibacterial effect, the anti-biofilm activity of B-Hydrogel was investigated. As shown in Fig. 5b, for the untreated biofilms, both of the MRSA and SA were stained with calcein-AM and emitted bright green fluorescence, while the biofilm formed a whole piece with dense and thick. By comparison, the whole biofilms were almost stained with red fluorescence PI for the B-Hydrogel treated group, and obvious damage on the bacterial biofilm could be observed (Fig. 5b). The statistics histogram of the bacterial biofilms also confirmed that the biofilm thickness of the B-Hydrogel treated group was significantly smaller than that of the untreated group, indicating the excellent anti-biofilm activity of B-Hydrogel (Fig. S9). Crystalline violet staining experiment also demonstrated that the bacterial biofilms were significantly reduced after B-Hydrogel treatment (Fig. S10). Overall, the developed B-Hydrogel not only has a significant killing effect on planktonic bacteria, but also possess a significant inhibitory effect on bacterial biofilms, showing excellent prominent antibacterial activity against common and resistant bacteria.

Good biocompatibility is an essential feature for biomaterials that can be used in living organisms, therefore, the biocompatibility of B-Hydrogel was explored. HUVECs, NIH-3T3, and HaCaT cells were selected as the model cells to evaluate the in vitro biocompatibility of B-Hydrogel. As shown in Fig. 5c, 5d and S11a, after treatment with B-Hydrogel for 12 h, the cell viabilities for the HUVECs, NIH-3T3, and HaCaT cells were almost the same as that of the control group. Even when the B-Hydrogel was co-incubated with the cells for 24 h, the survival rates of both types of cells were still greater than 92%. The fluorescence images of cell structure staining also confirmed that the microstructures of cells co-incubated with B-Hydrogel did not change significantly (Fig. 5e-f and Figs. S11a and S12), which was almost the same as that of blank cells. The B-Hydrogel almost have no obvious hemolysis to red blood cell (<8%), confirming the good blood compatibility (Fig. S13). Furthermore, the in vivo compatibility of the B-Hydrogel was evaluated by embedding the hydrogel in the skin surface of mice. The HE stained tissue sections displayed that there were no significant structural or morphological changes in the major organs (heart, liver, spleen, lung and kidney) of mice treated with B-Hydrogel for either a day or a week, which was almost the same as that of the normal mice (Fig. S14). These results demonstrated that the B-Hydrogel have excellent biocompatibility, showing significant application potential in vivo.

3.6. In vivo wound healing

Given the above excellent performance, we next evaluated the antibacterial potential and promoting wound healing of B-Hydrogel in

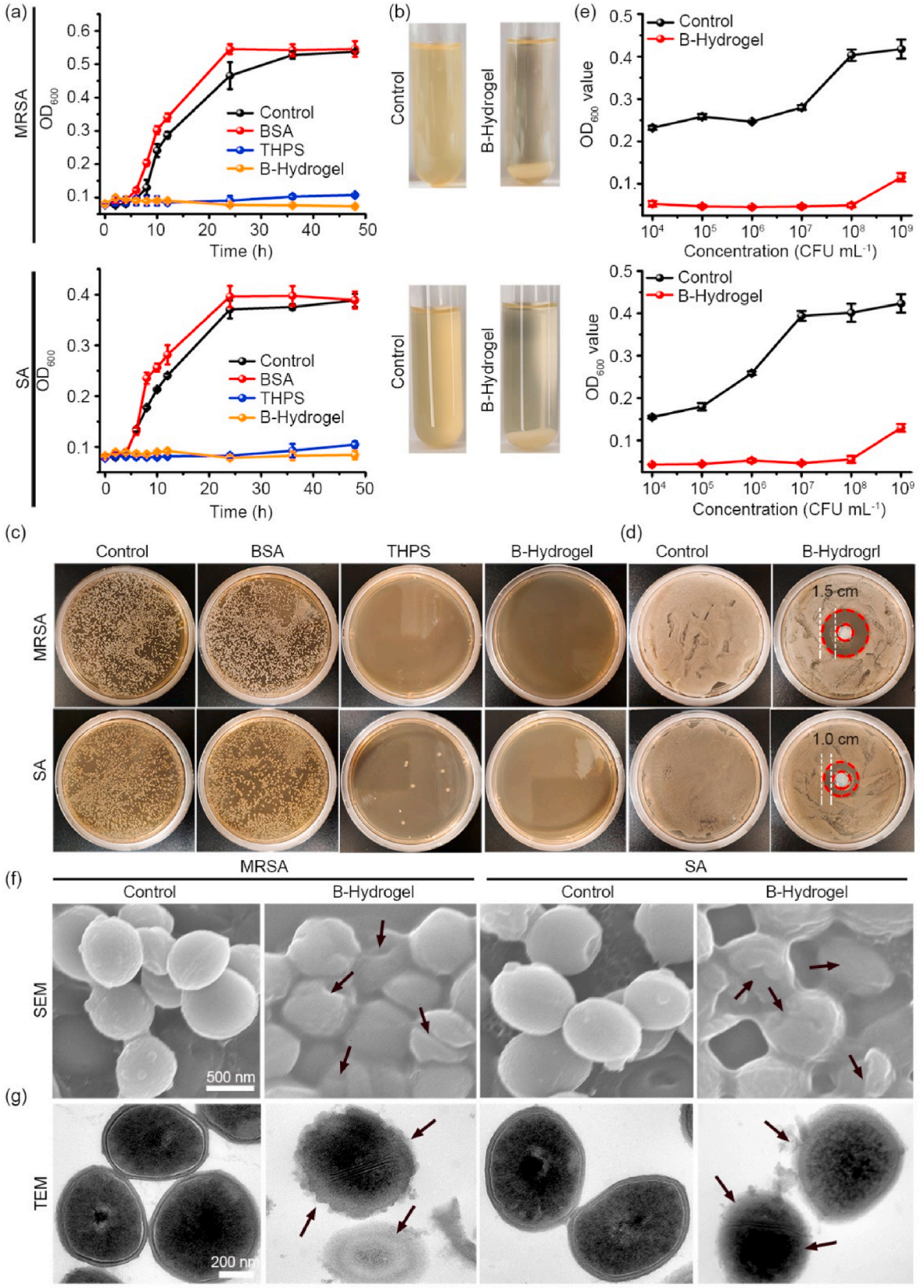

Fig. 4. (a) Growth curves of MRSA and SA with different treatments. (b) Photographs of MRSA and SA solution after B-Hydrogel treatment. (c) Photographs of MRSA and SA bacterial colonies grown on LB agar plates after various treatments. (d) MRSA and SA bacterial inhibition ring after treatment with B-Hydrogel. (e) Growth profiles of MRSA and SA bacteria with different concentration after co-incubation with the B-Hydrogel for 24 h. SEM images (f) and TEM images (g) of MRSA and SA after co-incubation with B-Hydrogel for 12 h (The arrows indicate damage to the bacterial cell membrane).

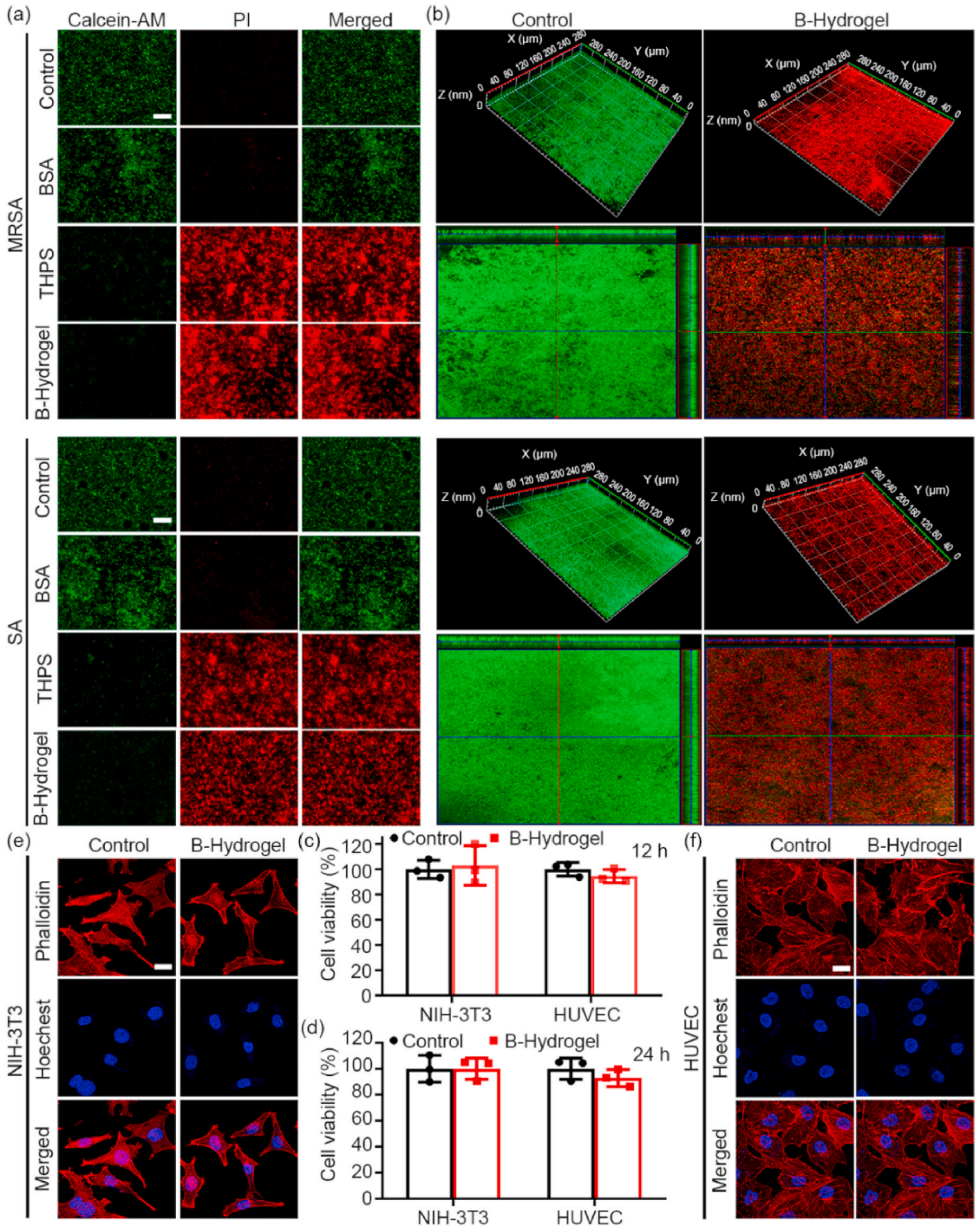

Fig. 5. (a) The membrane integrity of MRSA and SA bacteria were examined via calcein-AM/PI staining after various treatments. (Scale bar, 30 μm). (b) 3D fluorescent staining images (upper) and frontal 2D fluorescent images (lower) of MRSA and SA bacterial biofilms before and after treatment with B-Hydrogel (The lengths of red and green axis are 280 μm; The small boxes at the top and right side in the 2D fluorescent images represent biofilm thickness.). Cell viabilities of NIH-3T3 and HUVEC after co-incubation with B-Hydrogel for 12 h (c) and 24 h (d). Fluorescence staining images of NIH-3T3 (e) and HUVEC (f) after co-incubation with B-Hydrogel for 12 h (Scale bar, 60 μm). (For interpretation of the references to colour in this figure legend, the reader is referred to the Web version of this article.)

vivo through mouse model with infected wounds. The skin wounds infected mice were randomly divided into 4 groups: G1, control; G2, BSA; G3, THPS; G4, B-Hydrogel. Subsequently, the infected mice received the corresponding treatments above, and the infected wound were monitored over time to evaluate the wound healing effect. As shown in Fig. 6a, the wounds of mice in both G3 and G4 groups were nearly completely healed, and no obvious scabs were observed. Notably, compared with G3 group, the wound healing scars of mice in group G4 was slightly smaller than those in group G3 and exhibited the best wound healing, which may be attributed to the adhesiveness and moisture retention of B-Hydrogel that enabled it to have a more durable antibacterial effect and faster wound healing than THPS solution. In

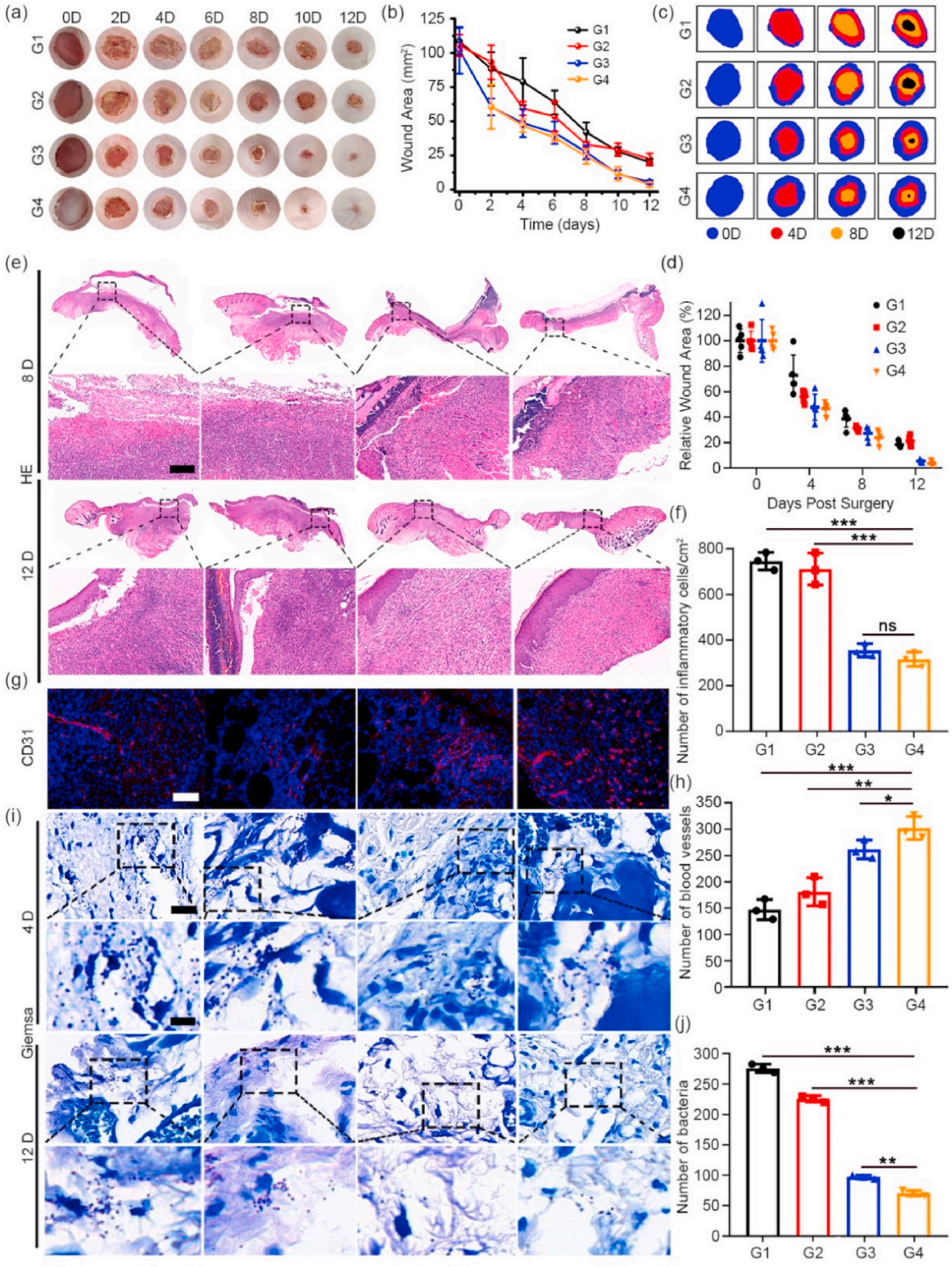

Fig. 6. (a) Images for the skin wound healing of MRSA infected mice after various treatments: G1, Control; G2, BSA; G3, THPS; and G4, B-Hydrogel. (b) Wound area profiles of mice after various treatments. (c) Schematic diagram of wound area during the wound healing. (d) Relative wound area for each group in (c). (e) Representative H&E staining images of mice wound at different times after different treatments (Scale bar, 60 μm). (f) Quantification of inflammatory cells in (e) after 12 d treatment. (g) CD31 (vascular biomarker) immunofluorescence staining for wound beds at 12 d treatment (Scale bar, 100 μm). (h) Quantitative analysis of neovascularization in (g). (i) Giemsa staining of wound beds after various time treatment (Upper, scale bar, 100 μm; Lower, scale bar, 200 μm). (j) Quantitative analysis of residual bacteria in (i) at 4 d treatment. *P < 0.05, **P < 0.01, and ***P < 0.001. ns, not statistically significant.

comparison, there were distinct wounds and scabs in the G1 and G2 groups, indicating the poor wound healing. The wound healing process and eventual wound closure in mice were also displayed in Fig. 6c. Moreover, the wound healing curves also verified the best wound healing in the G4 group, which was much faster than that of the G1 and G2 groups (Fig. 6b). The quantitative result of wound area ratio of B-Hydrogel treatment group is about 3.7% on day 12. By contrast, approximate 18.5% and 21.2% of wound area were remained for the G1 and G2 groups, respectively (Fig. 6d). All these results showed that the wound healing rate of B-Hydrogel treatment was faster than that of the other groups, demonstrating the excellent wound healing capacity of B-Hydrogel.

The hematoxylin and eosin (H&E) staining was executed to further investigate the wound healing process. On day 4, an obvious boundary between the wound and the normal tissue was observed for all the groups, while numerous inflammatory cells were observed in the groups of G1 and G2 (Fig. S15). In contrast, although there was also a clear dividing line between normal tissue and the wound, significantly fewer inflammatory cells in the G3 and G4 groups than the other groups were found (Fig. S15), which was likely attributed to the antimicrobial effect of THPS and B-Hydrogel. On day 8, no obvious epithelial structures in the wound sites of the G1 and G2 groups were observed, and the abundant of inflammatory cells was still found (Fig. 6e). Comparatively, for the group of G3 and G4, the epithelium and granulation structures in the G3 and G4 groups were denser, especially in the G4 group. Moreover, the number of inflammatory cells in G3 and G4 was obviously lower than in the G1 and G2 groups (Fig. 6e). On day 12, although the skin wound of mice in the groups of G1 and G2 showed a certain healing trend, the formed epithelial tissues were not closely connected with the granulation layers, and obvious separation was presented (Fig. 6e). More seriously, there were still excessive inflammation in the G1 and G2 groups (Fig. 6f), which is likely the main cause of delayed wound healing. The neutrophils staining also confirmed the existent of numerous inflammatory cells for the groups of G1 and G2 (Fig. S16). Conversely, for G3 and G4, no distinct separation was found for the epithelial tissues and granulation layers, and the inflammation levels were also significantly lower than in the G1 and G2 groups (Fig. 6f), which is consistent with the results of neutrophils staining (Fig. S16). Notably, the density of the formed granulation tissue in the G3 group was significantly looser than that in the G4 group (Fig. 6e), which may be due to the moisturizing property of the hydrogel, playing a certain role in promoting wound healing. The epithelium formed in the G4 group was also thicker than that formed in the G3 group (Fig. S17). Additionally, the neovascularization for the G3 and G4 groups were obvious more than G1 and G2 groups, while the formed microvessels for G4 group had the highest number of microvessels (Fig. 6g), which was also confirmed in the quantitative microvascular histogram (Fig. 6h).

Owing to the large number of microorganisms in the air environment, the skin wounds of mice exposed to air are prone to be breeding bacteria, which may delay wound healing. Moreover, the infected environment can also increase wound inflammation, further delaying wound healing. Therefore, Giemsa staining was employed to assess the bacterial infection of different groups. A large number of bacteria could be found in the wound bed of G1 and G2 on day 4, and the number was significantly higher than that of G3 and G4 (Fig. S18). With the advance of wound healing time, the number of bacteria in the wound beds of mice in all groups gradually decreased, but the number of bacteria in the G1 and G2 groups were always much higher than that in the G3 and G4 groups (Fig. 6i and j). At the endpoint, some bacteria still remained in the G1 and G2 groups, which also corresponded to poor wound healing in the G1 and G2 groups. In contrast, negligible staining bacteria were found in G3 and G4 groups (Fig. 6i), which was ascribed to the superior antibacterial property mediated by THPS and B-Hydrogel. Taken all together, our results suggested that the B-Hydrogel has the capacity of promoting wound healing through affording a moist atmosphere and releasing THPS to inhibit bacterial proliferation.

3.7. Clinical significance and limitations

As an alternative to traditional antibiotic therapy, hydrogel-based antibacterial therapy has attracted more and more attention in clinic. For hydrogels, they generally possess many merits, such as controllable and sustained-release, local drug delivery, enhanced mechanical properties and excellent biocompatibility, which are required by clinical antibacterial biomaterials. The developed protein-based antibacterial hydrogels also have the above advantages. Additionally, these protein-based hydrogels with excellent antibacterial activity not only can kill MRSA and SA, but also can destroy bacterial biofilms, overcoming biofilm-induced drug resistance. All of these advantages make the constructed protein-based hydrogels hold great potential in clinical MRSA disinfection.

Although these protein-based hydrogels have huge potential for clinical application, further research is needed, especially on their biodegradability and possible inflammatory responses, which will determine whether they can be used clinically. Additionally, THPS release is a key parameter mediating the antibacterial activity of these protein-based hydrogels, therefore, the release kinetics of THPS in different biological media should be assessed. The sterilization-mediated wound healing activity and biosafety of these protein-based hydrogels in large animals also need to be further explored, which can also provide important reference significance for subsequent possible clinical trials.

4. Conclusion

In summary, a general method for construction of antibiotic-free protein-based hydrogel with superior antibacterial activity to fight against drug-resistant bacteria and biofilm, as well as promote MRSA-infected wound healing was proposed. The hydrogel was synthesized via the Mannich reaction between the amino group in protein and the hydroxyl group in THPS to form an interpenetrating network structure through simple mixing without the introduction of any other initiator. Notably, this facile gel formation strategy can be applied to the gelation of at least ten different proteins, indicating the universality of this smart, simple and mild strategy. As one of the typical representatives, the B-Hydrogel not only exhibited excellent biocompatibility, but also had specific and strong antibacterial activity against MRSA and SA. The antibacterial mechanism demonstrated that this B-Hydrogel could release THPS to induce bacterial cell wall and membrane destruction, resulting in the bacteria's death. More importantly, this B-Hydrogel also could destroy bacterial biofilms, effectively overcoming the possibility that bacteria will develop resistance. Furthermore, the in vivo results demonstrated that this B-Hydrogel could serve as a wound dressing to accelerate the MRSA-infected wound healing through the elimination of MRSA, without causing obvious side effects. Therefore, this new protein-based hydrogel not only opens an avenue to provide a facile, feasible and general gelation strategy, but also has a broad application prospect in hospital and community MRSA disinfection and treatment.

CRediT authorship contribution statement

Jiang Ouyang: Conceptualization, Methodology, Writing – original draft. **Qingyue Bu:** Methodology, Writing – review & editing. **Na Tao:** Conceptualization, Methodology. **Mingkai Chen:** Writing – review & editing. **Haijun Liu:** Writing – review & editing. **Jun Zhou:** Writing – review & editing. **Jinggong Liu:** Methodology. **Bo Deng:** Methodology. **Na Kong:** Investigation, Validation. **Xingcai Zhang:** Writing – review & editing, Validation. **Tianfeng Chen:** Resources, Methodology, Writing – review & editing, Supervision. **Yihai Cao:** Writing – review & editing. **Wei Tao:** Resources, Writing – review & editing, Validation, Supervision.

Declaration of interests

The authors declare that they have no known competing financial interests or personal relationships that could have appeared to influence the work reported in this paper.

Acknowledgments

This work is supported by Harvard Medical School/Brigham and Women's Hospital Department of Anesthesiology-Basic Scientist Grant (No. 2420 BPA075, W.T.), and Center for Nanomedicine Research Fund (No. 2019A014810, W.T.), Gillian Reny Stepping Strong Center for Trauma Innovation Breakthrough Innovator Award (No. 113548, W.T.), Nanotechnology Foundation (No. 2022A002721, W.T.), Farokhzad Family Distinguished Chair Foundation (W.T.), Khoury Innovation Award (No. 2020A003219, W.T.), and American Heart Association (AHA) Collaborative Sciences Award (No. 2018A004190, W.T.). J. O. was supported by the China Postdoctoral Science Foundation (No. 2020M683173).

Appendix A. Supplementary data

Supplementary data to this article can be found online at https://doi.org/10.1016/j.bioactmat.2022.03.033.

References

[1] W. Liu, W. Ou-Yang, C. Zhang, Q. Wang, X. Pan, P. Huang, C. Zhang, Y. Li, D. Kong, W. Wang, Synthetic polymeric antibacterial hydrogel for methicillin-resistant staphylococcus aureus-infected wound healing: nanoantimicrobial self-assembly, drug-and cytokine-free strategy, ACS Nano 14 (2020) 12905–12917, https://doi.org/10.1021/acsnano.0c03855.

[2] D. Gan, T. Xu, W. Xing, X. Ge, L. Fang, K. Wang, F. Ren, X. Lu, Mussel-inspired contact-active antibacterial hydrogel with high cell affinity, toughness, and recoverability, Adv. Funct. Mater. 29 (2019) 1805964, https://doi.org/10.1002/adfm.201805964.

[3] Y. Zhao, Z. Zhang, Z. Pan, Y. Liu, Advanced bioactive nanomaterials for biomedical applications, Explorations 1 (2021) 20210089, https://doi.org/10.1002/EXP.20210036.

[4] J. Ouyang, R.-Y. Liu, W. Chen, Z. Liu, Q. Xu, K. Zeng, L. Deng, L. Shen, Y.-N. Liu, A black phosphorus based synergistic antibacterial platform against drug resistant bacteria, J. Mater. Chem. B 6 (2018) 6302–6310, https://doi.org/10.1039/C8TB01669K.

[5] X. Yan, W.-W. Fang, J. Xue, T.-C. Sun, L. Dong, Z. Zha, H. Qian, Y.-H. Song, M. Zhang, X. Gong, Y. Lu, T. He, Thermoresponsive in situ forming hydrogel with sol–gel irreversibility for effective methicillin-resistant staphylococcus aureus infected wound healing, ACS Nano 13 (2019) 10074–10084, https://doi.org/10.1021/acsnano.9b02845.

[6] J. Wang, X.-Y. Chen, Y. Zhao, Y. Yang, W. Wang, C. Wu, B. Yang, Z. Zhang, L. Zhang, Y. Liu, X. Du, W. Li, L. Qiu, P. Jiang, X.-Z. Mou, Y.-Q. Li, pH-switchable antimicrobial nanofiber networks of hydrogel eradicate biofilm and rescue stalled healing in chronic wounds, ACS Nano 13 (2019) 11686–11697, https://doi.org/10.1021/acsnano.9b05608.

[7] H. Haidari, Z. Kopecki, R. Bright, A.J. Cowin, S. Garg, N. Goswami, K. Vasilev, Ultrasmall agnp-impregnated biocompatible hydrogel with highly effective biofilm elimination properties, ACS Appl. Mater. Interfaces 12 (2020) 41011–41025, https://doi.org/10.1021/acsami.0c09414.

[8] S. Li, S. Dong, W. Xu, S. Tu, L. Yan, C. Zhao, J. Ding, X. Chen, Antibacterial hydrogels, Adv. Sci. 5 (2018) 1700527, https://doi.org/10.1002/advs.201700527.

[9] C. Feng, J. Ouyang, Z. Tang, N. Kong, Y. Liu, L. Fu, X. Ji, T. Xie, O.C. Farokhzad, W. Tao, Germanene-based theranostic materials for surgical adjuvant treatment: inhibiting tumor recurrence and wound infection, Matter 3 (2020) 127–144, https://doi.org/10.1016/j.matt.2020.04.022.

[10] Z. Chen, Z. Lv, Z. Zhang, D.A. Weitz, H. Zhang, Y. Zhang, W. Cui, Advanced microfluidic devices for fabricating multi-structural hydrogel microsphere, Explorations 1 (2021) 20210036, https://doi.org/10.1002/EXP.20210089.

[11] C. Cao, N. Yang, Y. Zhao, D. Yang, Y. Hu, D. Yang, X. Song, W. Wang, X. Dong, Biodegradable hydrogel with thermo-response and hemostatic effect for photothermal enhanced anti-infective therapy, Nano Today 39 (2021) 101165, https://doi.org/10.1016/j.nantod.2021.101165.

[12] M.U. Hashmi, F. Khan, N. Khalid, A.A. Shahid, A. Javed, T. Alam, N. Jalal, M. Q. Hayat, S.R. Abbas, H.A. Janjua, Hydrogels incorporated with silver nanocolloids prepared from antioxidant rich aerva javanica as disruptive agents against burn wound infections, Colloids Surf., A 529 (2017) 475–486, https://doi.org/10.1016/j.colsurfa.2017.06.036.

[13] H. Haidari, R. Bright, S. Garg, K. Vasilev, A.J. Cowin, Z. Kopecki, Eradication of mature bacterial biofilms with concurrent improvement in chronic wound healing using silver nanoparticle hydrogel treatment, Biomedicines 9 (2021) 1182, https://doi.org/10.3390/biomedicines9091182.

[14] H. Haidari, R. Bright, X.L. Strudwick, S. Garg, K. Vasilev, A.J. Cowin, Z. Kopecki, Multifunctional ultrasmall AgNP hydrogel accelerates healing of S. aureus infected wounds, Acta Biomater. 128 (2021) 420–434, https://doi.org/10.1016/j.actbio.2021.04.007.

[15] M.I. Khan, P. Paul, S.K. Behera, B. Jena, S.K. Tripathy, C.S. Lundborg, A. Mishra, To decipher the antibacterial mechanism and promotion of wound healing activity by hydrogels embedded with biogenic Ag@ZnO core-shell nanocomposites, Chem. Eng. J. 417 (2021) 128025, https://doi.org/10.1016/j.cej.2020.128025.

[16] M. Ribeiro, M.P. Ferraz, F.J. Monteiro, M.H. Fernandes, M.M. Beppu, D. Mantione, H. Sardon, Antibacterial silk fibroin/nanohydroxyapatite hydrogels with silver and gold nanoparticles for bone regeneration, Nanomed. Nanotechnol. Biol. Med. 13 (2017) 231–239, https://doi.org/10.1016/j.nano.2016.08.026.

[17] C. Bermúdez-Jiménez, M.G. Romney, S.A. Roa-Flores, G. Martínez-Castañón, H. Bach, Hydrogel-embedded gold nanorods activated by plasmonic photothermy with potent antimicrobial activity, Nanomed. Nanotechnol. Biol. Med. 22 (2019) 102093, https://doi.org/10.1016/j.nano.2019.102093.

[18] T. Dai, C. Wang, Y. Wang, W. Xu, J. Hu, Y. Cheng, A nanocomposite hydrogel with potent and broad-spectrum antibacterial activity, ACS Appl. Mater. Interfaces 10 (2018) 15163–15173, https://doi.org/10.1021/acsami.8b02527.

[19] M. Choi, N. Hasan, J. Cao, J. Lee, S.P. Hlaing, J.-W. Yoo, Chitosan-based nitric oxide-releasing dressing for anti-biofilm and in vivo healing activities in mrsa biofilm-infected wounds, Int. J. Biol. Macromol. 142 (2020) 680–692, https://doi.org/10.1016/j.ijbiomac.2019.10.009.

[20] Y. Wan, L. Liu, S. Yuan, J. Sun, Z. Li, pH-responsive peptide supramolecular hydrogels with antibacterial activity, Langmuir 33 (2017) 3234–3240, https://doi.org/10.1021/acs.langmuir.6b03986.

[21] X. Jiang, M. Li, X. Guo, H. Chen, M. Yang, A. Rasooly, Self-assembled DNA-thps hydrogel as a topical antibacterial agent for wound healing, ACS Appl. Bio. Mater. 2 (2019) 1262–1269, https://doi.org/10.1021/acsabm.8b00818.

[22] T. Xia, X. Jiang, L. Deng, M. Yang, X. Chen, Albumin-based dynamic double cross-linked hydrogel with self-healing property for antimicrobial application, Colloids Surf., B (2021) 112042, https://doi.org/10.1016/j.colsurfb.2021.112042.

[23] M. Olkiewicz, M.P. Caporgno, J. Font, J. Legrand, O. Lepine, N.V. Plechkova, J. Pruvost, K.R. Seddon, C. Bengoa, A novel recovery process for lipids from microalgæ for biodiesel production using a hydrated phosphonium ionic liquid, Green Chem. 17 (2015) 2813–2824, https://doi.org/10.1039/C4GC02448F.

[24] X. Guo, J. Yang, Y. Liang, J. Liu, B. Xiao, Evaluation of sludge reduction by an environmentally friendly chemical uncoupler in a pilot-scale anaerobic/anoxic/oxic process, Bioproc. Biosyst. Eng. 37 (2014) 553–560, https://doi.org/10.1007/s00449-013-1022-3.

[25] R. Jia, Y. Li, H.H. Al-Mahamedh, T. Gu, Enhanced biocide treatments with D-amino acid mixtures against a biofilm consortium from a water cooling tower, Front. Microbiol. 8 (2017) 1538, https://doi.org/10.3389/fmicb.2017.01538.

[26] P. Li, H. Li, J. Li, X. Guo, J. Liu, B. Xiao, Evaluation of sludge reduction of three metabolic uncouplers in laboratory-scale anaerobic–anoxic–oxic process, Bioresour. Technol. 221 (2016) 31–36, https://doi.org/10.1016/j.biortech.2016.09.019.

[27] D. Xu, J. Wen, W. Fu, T. Gu, I. Raad, D-amino acids for the enhancement of a binary biocide cocktail consisting of thps and edds against an srb biofilm, World J. Microbiol. Biotechnol. 28 (2012) 1641–1646, https://doi.org/10.1007/s11274-011-0970-5.

[28] T. Connor, J. Meyne, M. Legator, The mutagenic evaluation of tetrakis (hydroxymethyl) phosphonium sulfate using a combined testing protocol approach, J. Environ. Pathol. Toxicol. 4 (1980) 145–158. https://europepmc.org/article/med/7003047.

[29] B. Downward, R. Talbot, T. Haak, Tetrakis Hydroxymethyl Phosphonium Sulphate (THPS). A New Industrial Biocide with Low Environmental Toxicity, 401, 1997. New Orleans, https://onepetro.org/NACECORR/proceedings-abstract/CORR97/All-CORR97/NACE-97401/113535.

[30] W. Liu, J. Sun, Y. Sun, Y. Xiang, Y. Yan, Z. Han, W. Bi, F. Yang, Q. Zhou, L. Wang, Multifunctional injectable protein-based hydrogel for bone regeneration, Chem. Eng. J. 394 (2020) 124875, https://doi.org/10.1016/j.cej.2020.124875.

[31] A. Upadhyay, R. Kandi, C.P. Rao, Injectable, self-healing, and stress sustainable hydrogel of BSA as a functional biocompatible material for controlled drug delivery in cancer cells, ACS Sustain. Chem. Eng. 6 (2018) 3321–3330, https://doi.org/10.1021/acssuschemeng.7b03485.

[32] C.S. Kim, Y.J. Yang, S.Y. Bahn, H.J. Cha, A bioinspired dual-crosslinked tough silk protein hydrogel as a protective biocatalytic matrix for carbon sequestration, NPG Asia Mater. 9 (2017), https://doi.org/10.1038/am.2017.71 e391-e391.

[33] J. Ouyang, X. Ji, X. Zhang, C. Feng, Z. Tang, N. Kong, A. Xie, J. Wang, X. Sui, L. Deng, Y. Liu, J.S. Kim, Y. Cao, W. Tao, In situ sprayed nir-responsive, analgesic black phosphorus-based gel for diabetic ulcer treatment, P. Natl. Acad. Sci. USA 117 (2020) 28667–28677, https://doi.org/10.1073/pnas.2016268117.

[34] J. Ouyang, C. Feng, X. Zhang, N. Kong, W. Tao, Black phosphorus in biological applications: evolutionary journey from monoelemental materials to composite materials, Acc. Mater. Res. 2 (2021) 489–500, https://doi.org/10.1021/accountsmr.1c00039.

[35] C. Chung, K.J. Lampe, S.C. Heilshorn, Tetrakis (hydroxymethyl) phosphonium chloride as a covalent cross-linking agent for cell encapsulation within protein-based hydrogels, Biomacromolecules 13 (2012) 3912–3916, https://doi.org/10.1021/bm3015279.

[36] H. Peng, W.-H. Zhang, W.-S. Hung, N. Wang, J. Sun, K.-R. Lee, Q.-F. An, C.-M. Liu, Q. Zhao, Phosphonium modification leads to ultrapermeable antibacterial

polyamide composite membranes with unreduced thickness, Adv. Mater. 32 (2020), 2001383, https://doi.org/10.1002/adma.202001383.
[37] C. Chung, K.J. Lampe, S.C. Heilshorn, Tetrakis(hydroxymethyl) phosphonium chloride as a covalent cross-linking agent for cell encapsulation within protein-based hydrogels, Biomacromolecules 13 (2012) 3912–3916, https://doi.org/10.1021/bm3015279.
[38] S. Tian, L. Su, Y. Liu, J. Cao, G. Yang, Y. Ren, F. Huang, J. Liu, Y. An, H.C. van der Mei, Self-targeting, zwitterionic micellar dispersants enhance antibiotic killing of infectious biofilms-An intravital imaging study in mice, Sci. Adv. 6 (2020), https://doi.org/10.1126/sciadv.abb1112 eabb1112.
[39] J. Ouyang, M. Wen, W. Chen, Y. Tan, Z. Liu, Q. Xu, K. Zeng, L. Deng, Y.-N. Liu, Multifunctional two dimensional Bi_2Se_3 nanodiscs for combined antibacterial and anti-inflammatory therapy for bacterial infections, Chem. Commun. 55 (2019) 4877–4880, https://doi.org/10.1039/C9CC01129C.
[40] L. Xia, J. Tian, T. Yue, H. Cao, J. Chu, H. Cai, W. Zhang, Pillar[5]arene-Based acid-triggered supramolecular porphyrin photosensitizer for combating bacterial infections and biofilm dispersion, Adv. Healthc. Mater. 11 (2022) 2102015, https://doi.org/10.1002/adhm.202102015.
[41] F. Yu, C. Chen, G. Yang, Z. Ren, H. Cao, L. Zhang, W. Zhang, An acid-triggered porphyrin-based block copolymer for enhanced photodynamic antibacterial efficacy, Sci. China Chem. 64 (2021) 459–466, https://doi.org/10.1007/s11426-020-9904-7.
[42] A.D. Verderosa, M. Totsika, K.E. Fairfull-Smith, Bacterial biofilm eradication agents: a current review, Front. Chem. 7 (2019) 824, https://doi.org/10.3389/fchem.2019.00824.
[43] J. Berman, D.J. Krysan, Drug resistance and tolerance in fungi, Nat. Rev. Microbiol. 18 (2020) 319–331, https://doi.org/10.1038/s41579-019-0322-2.